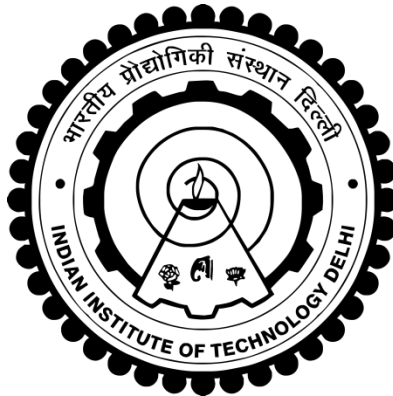


**ANALYSIS, DESIGN AND CONTROL OF DOUBLY FED  
INDUCTION GENERATOR FOR WIND ENERGY  
CONVERSION SYSTEMS**

**N KRISHNA SWAMI NAIDU**



**DEPARTMENT OF ELECTRICAL ENGINEERING  
INDIAN INSTITUTE OF TECHNOLOGY DELHI  
HAUZ KHAS, NEW DELHI – 110016, INDIA  
MAY 2015**

© Indian Institute of Technology Delhi (IITD), New Delhi, 2015

**ANALYSIS, DESIGN AND CONTROL OF DOUBLY FED  
INDUCTION GENERATOR FOR WIND ENERGY  
CONVERSION SYSTEMS**

by

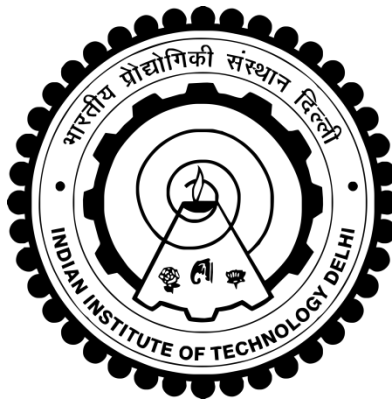
**N KRISHNA SWAMI NAIDU**  
**Electrical Engineering Department**

*Submitted*

*in fulfillment of the requirements of the degree of*

**DOCTOR OF PHILOSOPHY**

to the



**INDIAN INSTITUTE OF TECHNOLOGY DELHI**

**MAY 2015**

# **CERTIFICATE**

It is certified that the thesis entitled “**Analysis, Design and Control of Doubly Fed Induction Generators for Wind Energy Conversion Systems,**” being submitted by **Mr. N Krishna Swami Naidu** for award of the degree of **Doctor of Philosophy** in the Department of Electrical Engineering, Indian Institute of Technology Delhi, is a record of the student work carried out by him under my supervision and guidance. The matter embodied in this thesis has not been submitted for award of any other degree or diploma.

**(Prof. Bhim Singh)**

**Department of Electrical Engineering  
Indian Institute of Technology Delhi  
Hauz Khas, New Delhi-110016, India**

**Date:**

**Place:**

## ACKNOWLEDGEMENTS

I wish to express my deepest gratitude and indebtedness to **Prof. Bhim Singh** for providing me an opportunity to carry out the Ph.D. work under his supervision. His keenness and vision have played an important role in guiding me throughout this study. Working under him has been a wonderful experience, which has provided a deep insight to the world of research. Determination, dedication, innovativeness, resourcefulness and discipline of **Prof. Bhim Singh** have been the inspiration for me to complete this work. His consistent encouragement, continuous monitoring and commitments to excellence have always motivated me to improve my work and use the best of my capabilities.

My sincere thanks and deep gratitude to **Prof. T.S. Bhatti, Prof. G. Bhuvanewari,** and **Prof. Sukumar Mishra**, all SRC members for their valuable guidance and consistent support during my research work.

I wish to convey my sincere thanks to **Prof. Bhim Singh, Prof. B. P. Singh, Prof. T.S. Bhatti, Prof. Sukumar Mishra** and **Dr. Amit Kumar Jain** for their valuable inputs during my course work which helped me to enrich my knowledge. I am grateful to IIT Delhi for providing me the research facilities. I would wish to express my sincere gratitude to **Prof. K. R. Rajagopal**, Prof. in-charge, PG Machine Lab., for providing me immense facilities to carry out experimental work. I am too grateful to **Prof. G. Bhuvanewari**, Prof. in-charge, Power Electronics Lab for her whole hearted support in my research work. Thanks are due to Sh. Srichand, Sh. Puran Singh, Sh. Dhan Raj Singh, Sh. Jagbir Singh, Sh. Gurcharan Singh, Sh. Satey Singh Negi of PG Machines Lab, UG Machines Lab, Workshop and Power Electronics Lab., IIT Delhi for providing me the facilities and assistance during this work.

I would like to offer my sincere thanks to Dr. Shailendra Sharma and Dr. V. Raja Gopal who have endorsed me during initial start-up of my research work. I am extremely grateful to all my friends and well-wishers, particularly I would like to extend my sincere thanks to Dr. Ashish Shrivastava, Dr. V. Sandeep, Dr. Rajashekhar Reddy, Dr. Jeevanand Seshadrinath, Dr. Rajesh Mutharath, Dr. Sabharaj Arya, Mr. Arun Kumar Verma, Mr. Subir Karmakar, Mr. Ram Niwas, Mr. Ujjwala Kalla, Mr. Raj Kumar Garg, Mr. Phaneendra Babu Bobba, Mr. Sathish Bhogineni, Mr. Gaurang Vakil, Mr. P. Chandra Sekhar, Mr. Bharath Babu Ambati, Ms. Pavani Nerella, Mr. Subrat Kumar, Dr. Shikha Singh, Ms. Swati Narula, Mr. Aman Jha, Mr. Sangram Keshri Nayak, Mr. Shailendra Tiwari, Mrs. Geetha Pathak, Mr. Rajan Kumar Sonkar and Mr. Ikhlq Bohru for their valuable aid and co-operation. My sincere thanks are due to Mr. Madishetti Sandeep, Mr. Vashist Bisht and Mr. Chinmay Jain for co-operation and informal support in pursuing experimental work. My sincere and special thanks to Mr. Sandeep Madishetti for his support and co-operation throughout my stay in IIT Delhi. I am likewise thankful to those who directly or indirectly helped me to finish my dissertation study.

My deepest love, appreciation and indebtedness go to my parents Mr. N. Badrachala Rama Govinda and Mrs. Surya Demudu for their ambitions, sacrifices and whole hearted support. I must appreciate my sisters Ms. Kalyani and Ms. Sobha Rani always behind me to provide the moral support for achieving this academic level.

At last, I am beholden to almighty for their blessings to help me to raise my academic level to this stage. I pray for their benediction in my future endeavors. Their blessings may be showered on me for strength, wisdom and determination to achieve in future.

Date:

N Krishna Swami Naidu

## **ABSTRACT**

Population growth and industrialization are the main reasons for the exponential increase in the electrical power demand. The major sources of the power generation are fossil fuels like coal, petroleum and gas which are depleting at a faster rate. The major concerns with these fossil fuels are the greenhouse emissions which in turn leads to climate change. Therefore, there is need to increase in the power generation from the renewable energy sources like solar, wind and bio mass. With latest technological advancements, wind energy is becoming the cheapest among all renewable energy sources. Doubly fed induction generators (DFIGs) are typically used as a variable speed wind energy conversion systems (WECSs) due to the reduction in the size of the power converters and also the converter losses. Therefore, this DFIG based WECS has the share about 50% of the total installed WECS all over the world. The DFIG based variable speed grid interfaced WECS are used for the power generation.

Normally, the voltage at the remote locations is not regulated at the desired value. This research aims the voltage regulation at the remote locations with the proper control of DFIG without adding any extra reactive power compensators. Attempts are made for achieving voltage regulation at the grid by the coordinated control of rotor side converter (RSC) and grid side converter (GSC) in addition to the conventional DFIG functionalities such as maximum power point tracking, decoupled control of active and reactive powers.

This research work also aims to investigate the solutions for volatile power generation from the grid connected WECS and also the power quality problems at the grid. The variation in the power generation prevails when the wind energy penetration increases in the total power due to its intermittent nature of wind. Therefore battery energy storage systems (BESS) is integrated with DFIG based grid connected WECS for smoothening the power and also for regulating the power

feeding to the grid irrespective of the wind speed. Attempts are also made for achieving the regulated power output by modifying the control algorithm of the GSC and also by the proper selection of BESS using the wind data of the proposed system.

A new topology of grid connected DFIG based WECS is investigated by removing the GSC and by integrating BESS in the DC link of RSC. The advantages of single voltage source converter (VSC) based DFIG are compared with the conventional double VSC based DFIG. Investigations are made on the proposed single VSC based DFIG using vector control and direct power control algorithms for the variations in the wind speed. Attempts are made for eliminating the rotor position sensor to improve the reliability and to reduce the cost. The stator flux based model reference adaptive system control and simple position sensorless algorithms are used for estimating rotor position and speed of the DFIG.

Poor power quality is another major concern for the consumers as well as generating companies. Investigations are made for improving power quality in the distribution system with DFIG based WECS. Harmonic mitigation of loads connected at PCC has been achieved by modifying the control algorithm of GSC of DFIG based WECS. Working of this DFIG as an active filter is proposed even at wind turbine stalling condition. A grid connected DFIG with BESS is also verified for both power smoothening and active filter capabilities without adding any extra power electronics component.

Detailed performance of all these configurations of grid connected DFIG based WECS for the power quality improvement are verified by the developed prototype in the laboratory using digital signal processor (DSP-dSPACE DS1103) based controller. The proposed control algorithms of DFIG are validated on a developed prototype for the dynamic changes in wind speeds.

Still there are some areas, where the electricity through the grid connection is not feasible due to geo-graphic and economic constraints. In this research work, DFIG is also used for feeding standalone consumer loads. DFIG based standalone WECS is investigated under variety of consumer loads such as linear, nonlinear and dynamic loads. A mechanical sensorless algorithm is used for estimating the rotor position and speed. DFIG based SWECS is investigated with and without BESS. A prototype of the DFIG based SWECS is developed to demonstrate the performance under different variety of loads at varying wind speeds. The performance of this DFIG based SWECS is observed for maximum power point tracking, load leveling, load balancing, a neutral current compensation and harmonic elimination while feeding different types of loads.

# TABLE OF CONTENTS

		Page No.
	Certificate	i
	Acknowledgements	ii
	Abstract	iv
	Table of Contents	viii
	List of Figures	xv
	List of Tables	xxvi
	List of Abbreviations	xxvii
	List of Symbols	xxviii
<b>CHAPTER I</b>	<b>INTRODUCTION</b>	1-8
1.1	General	1
1.2	State of Art on DFIG Based WECS	2
1.3	Scope of Work	6
1.4	Outline of Chapters	8
<b>CHAPTER II</b>	<b>LITERATURE REVIEW</b>	12-25
2.1	General	12
2.2	Literature Survey	12
2.2.1	DFIG for Grid Interfaced WECS	14
2.2.1.1	DFIG for Grid Interfaced WECS With BESS for Power Smoothing	16
2.2.1.2	DFIG for Grid Interfaced WECS With Active Filtering Capabilities	18
2.2.2	Single VSC Based DFIG for Grid Interfaced WECS With BESS	19
2.2.3	DFIG for Standalone WECS	21
2.2.4	DFIG for Standalone WECS with BESS	22
2.2.5	Single VSC Based DFIG for Standalone WECS with BESS	23
2.3	Identified Research Areas	24
2.4	Conclusions	24
<b>CHAPTER III</b>	<b>ANALYSIS, DESIGN AND IMPLEMENTATION OF SINGLE VSC BASED DFIG FOR GRID INTERFACED WECS</b>	26-81
3.1	General	26
3.2	System Configuration of Single VSC Based DFIG for Grid Interfaced WECS	26
3.3	Design of Single VSC Based DFIG for Grid Interfaced WECS	27
3.3.1	Design and Selection of Wind Turbine	27
3.3.2	Design and Selection of Battery Voltage	28
3.3.3	Design and Selection of Battery Energy Storage System	29
3.3.4	Design and Selection of VSC	30
3.4	Control Algorithms for Single VSC Based DFIG for Grid Interfaced WECS	30
3.4.1	Vector Control Algorithm for RSC	30

3.4.2	Stator Flux MRAS Based Rotor Position Sensorless Algorithm	35
3.4.3	Direct Power Control Algorithm for RSC	36
3.4.4	Simple Position Sensorless Algorithm for Rotor Position Estimation	40
3.5	MATLAB Based Modelling of Single VSC Based DFIG for Grid Interfaced WECS	43
3.5.1	MATLAB Based Modelling of Single VSC Based DFIG for Grid Interfaced WECS with Vector Control Algorithm	44
3.5.2	MATLAB Based Modelling of Single VSC Based DFIG for Grid Interfaced WECS with DPC Algorithm	45
3.6	Hardware Implementation of Single VSC Based Grid Interfaced DFIG for WECS	48
3.6.1	DSP dSPACE DS1103 Controller	48
3.6.2	Interfacing Circuit for Hall Effect Voltage Sensors	49
3.6.3	Interfacing Circuit for Hall Effect Current Sensors	50
3.6.4	Rotor Position Estimation using Encoder	52
3.6.5	Interfacing Circuit for opto-couplers	52
3.7	Results and Discussion	54
3.7.1	Simulated Performance of Single VSC Based DFIG for Grid Interfaced WECS with Vector Control Algorithm	55
3.7.1.1	Steady State Performance of Single VSC Based DFIG for Grid Interfaced WECS with Vector Control Algorithm	55
3.7.1.2	Dynamic Performance of Single VSC Based DFIG for Grid Interfaced WECS with Vector Control Algorithm	58
3.7.2	Experimental Performance of Single VSC Based DFIG for Grid Interfaced WECS with Vector Control Algorithm	60
3.7.2.1	Steady State Performance of Single VSC Based DFIG for Grid Interfaced WECS with Vector Control Algorithm	60
3.7.2.2	Dynamic Performance of Single VSC Based DFIG for Grid Interfaced WECS with Vector Control Algorithm	63
3.7.3	Simulated Performance of Single VSC Based DFIG for Grid Interfaced WECS with DPC Algorithm	65
3.7.3.1	Steady State Performance of Single VSC Based DFIG for Grid Interfaced WECS with DPC Algorithm	65
3.7.3.2	Dynamic Performance of Single VSC Based DFIG for Grid Interfaced WECS with DPC Algorithm	70
3.7.4	Experimental Performance of Single VSC Based DFIG for Grid Interfaced WECS with DPC Algorithm	72
3.7.4.1	Steady State Performance of Single VSC Based DFIG for Grid Interfaced WECS with DPC Algorithm	73
3.7.4.2	Dynamic Performance of Single VSC Based DFIG for Grid Interfaced WECS with DPC Algorithm	75
3.8	Conclusions	81
<b>CHAPTER IV</b>	<b>ANALYSIS, DESIGN AND IMPLEMENTATION OF DFIG FOR GRID INTERFACED WECS</b>	<b>82-119</b>
4.1	General	82
4.2	System Configuration of DFIG for Grid Interfaced WECS	82
4.3	Design of DFIG for Grid Interfaced WECS	83
4.3.1	Design and Selection of Wind Turbine	83

4.3.2	Design and Selection of DC Link Voltage	84
4.3.3	Design and Selection of Rating of VSCs	84
4.3.4	Design of AC Interface Inductors	85
4.4	Control Algorithm of DFIG for Grid Interfaced WECS	85
4.4.1	Control Algorithm for Rotor Side Converter	86
4.4.2	Control Algorithm for Grid Side Converter	88
4.5	MATLAB Based Modelling of DFIG for Grid Interfaced WECS	90
4.6	Hardware Implementation of DFIG for Grid Interfaced WECS	91
4.7	Results and Discussion	92
4.7.1	Simulated Performance of DFIG for Grid Interfaced WECS in UPF mode	92
4.7.1.1	Steady State Performance of DFIG for Grid Interfaced WECS in UPF mode	92
4.7.1.2	Dynamic Performance of DFIG for Grid Interfaced WECS at Varying Wind Speeds in UPF mode	93
4.7.2	Experimental Performance of DFIG for Grid Interfaced WECS in UPF mode	97
4.7.2.1	Steady State Performance of DFIG for Grid Interfaced WECS in UPF Mode	97
4.7.2.2	Dynamic Performance of DFIG for Grid Interfaced WECS at Varying Wind Speeds in UPF Mode	104
4.7.3	Simulated Performance of DFIG for Grid Interfaced WECS in Voltage Regulation Mode	106
4.7.3.1	Steady State Performance of DFIG for Grid Interfaced WECS in Voltage Regulation Mode	106
4.7.3.2	Dynamic Performance of DFIG for Grid Interfaced WECS at Varying Wind Speeds in Voltage Regulation Mode	108
4.7.4	Experimental Performance of DFIG for Grid Interfaced WECS in Voltage Regulation Mode	112
4.7.4.1	Steady State Performance of DFIG for Grid Interfaced WECS in Voltage Regulation Mode	112
4.7.4.2	Dynamic Performance of DFIG for Grid Interfaced WECS at Varying Wind Speeds in Voltage Regulation Mode	117
4.8	Conclusions	119

**CHAPTER V ANALYSIS, DESIGN AND IMPLEMENTATION OF DFIG BASED GRID INTERFACED WECS WITH BESS FOR POWER SMOOTHENING 120-148**

5.1	General	120
5.2	System Configuration of DFIG Based Grid Interfaced WECS With BESS for Power Smoothing	120
5.3	Design of DFIG Based Grid Interfaced WECS With BESS for Power Smoothing	121
5.3.1	Design and Selection of Wind Turbine	121
5.3.2	Design and Selection of Battery Voltage	122
5.3.3	Design and Selection of Battery Energy Storage System	123
5.3.4	Design and Selection of Rating of VSCs	125
5.3.5	Design of AC Interface Inductors	125

5.4	Control Algorithm of DFIG for Grid Interfaced WECS With BESS for Power Smoothing	126
5.4.1	Control Algorithm of Rotor Side Converter	126
5.4.2	Control Algorithm of Grid Side Converter	129
5.5	MATLAB Based Modelling of DFIG for Grid Interfaced WECS With BESS for Power Smoothing	130
5.6	Hardware Implementation of DFIG for Grid Interfaced WECS With BESS for Power Smoothing	131
5.7	Results and Discussion	132
5.7.1	Simulated Performance of DFIG for Grid Interfaced WECS With BESS for Power Smoothing	133
5.7.1.1	Steady State Performance of DFIG for Grid Interfaced WECS With BESS for Power Smoothing	133
5.7.1.2	Dynamic Performance of DFIG for Grid Interfaced WECS With BESS for Power Smoothing	134
5.7.2	Experimental Performance of DFIG for Grid Interfaced WECS With BESS for Power Smoothing	138
5.7.2.1	Steady State Performance of DFIG for Grid Interfaced WECS With BESS for Power Smoothing	138
5.7.2.2	Dynamic Performance of DFIG for Grid Interfaced WECS With BESS for Power Smoothing	145
5.8	Conclusions	148

**CHAPTER VI ANALYSIS, DESIGN AND IMPLEMENTATION OF GRID INTERFACED DFIG FOR WECS WITH ACTIVE FILTER CAPABILITIES** 149-179

6.1	General	149
6.2	System Configuration of DFIG Based Grid Interfaced WECS With Active Filter Capabilities	149
6.3	Design of DFIG Based Grid Interfaced WECS With Active Filter Capabilities	149
6.3.1	Design and Selection of Wind Turbine	150
6.3.2	Design and Selection of DC Link Voltage	150
6.3.3	Design and Selection of Rating of VSC	151
6.3.4	Design of AC Interface Inductors	151
6.4	Control Algorithm of DFIG Based Grid Interfaced WECS With Active Filter Capabilities	152
6.4.1	Control Algorithm of Rotor Side Converter	152
6.4.2	Control Algorithm of Grid Side Converter	155
6.5	MATLAB Based Modelling of DFIG Based Grid Interfaced WECS With Active Filter Capabilities	156
6.6	Hardware Implementation of DFIG Based Grid Interfaced WECS With Active Filter Capabilities	157
6.7	Results and Discussion	158
6.7.1	Simulated Performance of DFIG Based Grid Interfaced WECS With Active Filter Capabilities	159
6.7.1.1	Steady State Performance DFIG Based Grid Interfaced WECS With Active Filter Capabilities	159

6.7.1.2	Dynamic Performance of DFIG Based Grid Interfaced WECS With Active Filter Capabilities	166
6.7.2	Experimental Performance of DFIG Based Grid Interfaced WECS With Active Filter Capabilities	167
6.7.2.1	Steady State Performance of DFIG Based Grid Interfaced WECS With Active Filter Capabilities	167
6.7.2.2	Dynamic Performance of DFIG Based Grid Interfaced WECS With Active Filter Capabilities	174
6.8	Conclusions	179
<b>CHAPTER VII</b>	<b>ANALYSIS, DESIGN AND IMPLEMENTATION OF DFIG BASED GRID INTERFACED WECS WITH POWER SMOOTHENING AND ACTIVE FILTER CAPABILITIES</b>	<b>180-211</b>
7.1	General	180
7.2	System Configuration of DFIG Based Grid Interfaced WECS With Power Smoothing and Active Filter Capabilities	180
7.3	Design of DFIG Based Grid Interfaced WECS With Power Smoothing and Active Filter Capabilities	181
7.3.1	Design and Selection of Wind Turbine	181
7.3.2	Design and Selection of BESS Voltage	182
7.3.3	Design and Selection of Battery Energy Storage System	182
7.3.4	Design and Selection of Rating of VSCs	182
7.3.5	Design of AC Interface Inductors	183
7.4	Control Algorithm of DFIG Based Grid Interfaced WECS With Power Smoothing and Active Filter Capabilities	183
7.4.1	Control Algorithm of Rotor Side Converter	184
7.4.2	Control Algorithm of Grid Side Converter	186
7.5	MATLAB Based Modelling of DFIG Based Grid Interfaced WECS With Power Smoothing and Active Filter Capabilities	187
7.6	Hardware Implementation of DFIG Based Grid Interfaced WECS With Power Smoothing and Active Filter Capabilities	188
7.7	Results and Discussion	189
7.7.1	Simulated Performance of DFIG Based Grid Interfaced WECS With Power Smoothing and Active Filter Capabilities	190
7.7.1.1	Steady State Performance of DFIG Based Grid Interfaced WECS With Power Smoothing and Active Filter Capabilities	190
7.7.1.2	Dynamic Performance of DFIG Based Grid Interfaced WECS With Power Smoothing and Active Filter Capabilities at Varying Wind Speeds	198
7.7.2	Experimental Performance of DFIG Based Grid Interfaced WECS With Power Smoothing and Active Filter Capabilities	201
7.7.2.1	Steady State Performance of DFIG Based Grid Interfaced WECS With Power Smoothing and Active Filter Capabilities	201
7.7.2.2	Dynamic Performance of DFIG Based Grid Interfaced WECS With Power Smoothing and Active Filter Capabilities at Varying Wind Speeds	206
7.8	Conclusions	211

<b>CHAPTER VIII</b>	<b>ANALYSIS, DESIGN AND IMPLEMENTATION OF DFIG BASED STANDALONE WIND ENERGY CONVERSION SYSTEM</b>	<b>212-237</b>
8.1	General	212
8.2	System Configuration of DFIG Based SWECS	212
8.3	Design of DFIG Based SWECS	213
8.3.1	Design and Selection of Wind Turbine	213
8.3.2	Design and Selection of DC Link Voltage	213
8.3.3	Design and Selection of Rating of VSC	214
8.3.4	Design of AC Interfacing Inductors	215
8.4	Control Algorithm of DFIG Based SWECS	215
8.4.1	Control of Rotor Side Converter	216
8.4.2	Control of Load Side Converter	218
8.5	MATLAB Based Modelling of DFIG Based SWECS	219
8.6	Hardware Implementation and Operational Sequence of DFIG Based SWECS	220
8.7	Results and Discussion	222
8.7.1	Simulated Performance of DFIG Based SWECS	222
8.7.1.1	Simulated Performance of DFIG Based SWECS under Linear Loads	222
8.7.1.2	Simulated Performance of DFIG Based SWECS under Nonlinear Loads	222
8.7.2	Experimental Performance of DFIG Based SWECS	223
8.7.2.1	Experimental Performance of DFIG Based SWECS under Linear Loads	223
8.7.2.2	Experimental Performance of DFIG Based SWECS under Nonlinear Loads	231
8.7.2.3	Experimental Performance of DFIG Based SWECS under Dynamic Loads	236
8.7.2.4	Experimental Performance of DFIG Based SWECS under Varying Wind Speed	237
8.8	Conclusions	237
<b>CHAPTER IX</b>	<b>ANALYSIS, DESIGN AND IMPLEMENTATION OF SINGLE VSC BASED STANDALONE DFIG FOR WECS WITH BESS</b>	<b>239-256</b>
9.1	General	239
9.2	System Configuration of Single VSC Based DFIG for SWECS With BESS	239
9.3	Design of Single VSC Based DFIG for SWECS With BESS	239
9.3.1	Design and Selection of Wind Turbine	240
9.3.2	Design and Selection of BESS Voltage	240
9.3.3	Design and Selection of Battery Energy Storage System	241
9.3.4	Design and Selection of Rating of VSC	241
9.4	Control Algorithm of VFC for Single VSC Based DFIG for SWECS With BESS	242
9.5	MATLAB Based Modelling of VFC for Single VSC Based DFIG for SWECS With BESS	244
9.6	Hardware Implementation and Operational Sequence of Single VSC Based DFIG for SWECS With BESS	245
9.7	Results and Discussion	246

9.7.1	Simulated Performance of Single VSC Based DFIG for SWECS under Linear Loads	246
9.7.2	Experimental Performance of Single VSC Based DFIG for SWECS With BESS	249
9.8	Conclusions	256
<b>CHAPTER X</b>	<b>ANALYSIS, DESIGN AND IMPLEMENTATION OF DFIG BASED STANDALONE WIND ENERGY CONVERSION SYSTEM WITH BATTERY ENERGY STORAGE SYSTEM</b>	<b>257-287</b>
10.1	General	257
10.2	System Configuration of DFIG Based SWECS with BESS	257
10.3	Design of DFIG Based SWECS with BESS	257
10.3.1	Design and Selection of Wind Turbine	258
10.3.2	Design and Selection of Battery Voltage	258
10.3.3	Design and Selection of Battery Energy Storage System	259
10.3.4	Design and Selection of Rating of VSC	259
10.3.5	Design of AC Interface Inductors	260
10.4	Control Algorithms of VFC for DFIG Based SWECS with BESS	260
10.4.1	Control of Rotor Side Converter	261
10.4.2	Control of Load Side Converter	263
10.4.2	Model reference adaptive system based sensorless algorithm	264
10.5	MATLAB Based Modelling of DFIG Based SWECS with BESS	265
10.6	Hardware Implementation of DFIG Based SWECS with BESS	268
10.7	Results and Discussion	268
10.7.1	Simulated Performance of VFC for DFIG Based SWECS with BESS	269
10.7.1.1	Simulated Performance of DFIG Based SWECS with BESS under Linear Loads	269
10.7.1.2	Simulated Performance of DFIG Based SWECS with BESS under Nonlinear Loads	269
10.7.1.3	Simulated Performance of DFIG Based SWECS with BESS under Varying Wind Speeds	270
10.7.2	Experimental Performance of DFIG Based SWECS with BESS	273
10.7.2.1	Experimental Performance of DFIG Based SWECS with BESS under Linear Loads	275
10.7.2.2	Experimental Performance of DFIG Based SWECS with BESS under Nonlinear Loads	276
10.7.2.3	Experimental Performance of DFIG Based SWECS with BESS under Dynamic Loads	282
10.7.2.4	Experimental Performance of DFIG Based SWECS with BESS under Varying Wind Speeds	284
10.8	Conclusions	287
<b>CHAPTER XI</b>	<b>MAIN CONCLUSIONS AND SUGGESTION FOR FURTHER WORK</b>	<b>288-292</b>
11.1	General	288
11.2	Main Conclusions	289

11.3	Suggestions for Further Work	292
<b>REFERENCES</b>		293
<b>APPENDICES</b>		305-306
<b>LIST OF PUBLICATIONS</b>		307
<b>BIO DATA</b>		308

## LIST OF FIGURES

- Fig. 3.1 Proposed System Configuration of Single VSC based DFIG for grid interfaced WECS.
- Fig. 3.2 Wind turbine power - speed characteristics.
- Fig. 3.3 Vector control algorithm for the proposed single VSC based DFIG for grid interfaced WECS.
- Fig. 3.4 Enhanced Phase Locked Loop (EPLL).
- Fig. 3.5 Stator flux based sensorless MRAS algorithm.
- Fig. 3.6 Direct power control algorithm for the proposed single VSC based DFIG for grid interfaced WECS.
- Fig. 3.7 Voltage vectors and location of stator flux in rotor reference frame divided into sectors.
- Fig. 3.8 Switching states of real and reactive powers hysteresis control.
- Fig. 3.9 Phasor diagram for rotor position estimation scheme.
- Fig. 3.10 Schematic diagram of the simple position sensorless scheme.
- Fig. 3.11 MATLAB model of a single VSC based grid interfaced DFIG for WECS with vector control.
- Fig. 3.12 MATLAB model of a vector control algorithm used for RSC.
- Fig. 3.13 MATLAB model of a stator flux based sensorless MRAS algorithm used for rotor position estimation.
- Fig. 3.14 Matlab model of a single VSC based DFIG for WECS with DPC algorithm.
- Fig. 3.15 Matlab model of a DPC algorithm.
- Fig. 3.16 Matlab model of a simple position sensorless algorithm.
- Fig. 3.17 Photograph of developed prototype of grid interfaced DFIG based WECS.
- Fig. 3.18 Interfacing circuit for Hall Effect voltage sensors.
- Fig. 3.19 Interfacing circuit for voltage sensor.
- Fig. 3.20 Interfacing circuit for Hall Effect current sensors.
- Fig. 3.21 Interfacing circuit of current sensor card.
- Fig. 3.22 Interfacing Circuit for opto-coupler.
- Fig. 3.23 Hardware circuit for the opto-coupler.
- Fig. 3.24 Steady state Performance of proposed single VSC based DFIG for grid interfaced WECS at sub-synchronous speed (0.867 pu).
- Fig. 3.25 Steady state Performance of proposed single VSC based DFIG for grid interfaced WECS at synchronous speed (1 pu).
- Fig. 3.26 Steady state Performance of proposed single VSC based DFIG for grid interfaced WECS at super synchronous speed (1.24 pu).
- Fig. 3.27 Dynamic performance of proposed DFIG based WECS at varying wind speeds from 8 m/sec to 11.5 m/sec.
- Fig. 3.28 Steady state performance of the proposed WECS at fixed wind speed 8.4 m/sec and at a rotor speed of 1380 rpm. (a)  $v_{ab}$  and  $i_{sa}$  (b)  $v_{ab}$  and  $i_{sb}$  (c)  $v_{ab}$  and  $i_{sc}$  (d) Stator power ( $P_s$ ) (e)  $v_{dc}$  and  $i_{dcr}$  (f) harmonic spectra of  $v_{ab}$  (g) harmonic spectra of  $i_{sa}$  (h) harmonic spectra of  $i_{sb}$  (i) harmonic spectra of  $i_{sc}$ .
- Fig. 3.29 Steady state performance of the proposed WECS at fixed wind speed 9.15 m/sec and at a rotor speed of 1500 rpm (a)  $v_{ab}$  and  $i_{sa}$  (b)  $v_{ab}$  and  $i_{sb}$  (c)  $v_{ab}$  and  $i_{sc}$  (d)

- Stator power ( $P_s$ ) (e)  $v_{dc}$  and  $i_{dcr}$  (f) harmonic spectra of  $v_{ab}$  (g) harmonic spectra of  $i_{sa}$  (h) harmonic spectra of  $i_{sb}$  (i) harmonic spectra of  $i_{sc}$ .
- Fig. 3.30 Steady state performance of the proposed WECS at fixed wind speed 10.2 m/sec and at a rotor speed of 1670 rpm (a)  $v_{ab}$  and  $i_{sa}$  (b)  $v_{ab}$  and  $i_{sb}$  (c)  $v_{ab}$  and  $i_{sc}$  (d) Stator power ( $P_s$ ) (e)  $v_{dc}$  and  $i_{dcr}$  (f) harmonic spectra of  $v_{ab}$  (g) harmonic spectra of  $i_{sa}$  (h) harmonic spectra of  $i_{sb}$  (i) harmonic spectra of  $i_{sc}$ .
- Fig. 3.31 Dynamic performance of proposed DFIG based WECS under rise in wind speed, (a)  $v_w$ ,  $\omega_r^*$ ,  $\omega_r$  and  $P_s$ , (b)  $i_{dr}^*$ ,  $i_{dr}$ ,  $i_{qr}^*$  and  $i_{qr}$ , (c)  $v_w$ ,  $i_{dr}^*$ ,  $i_{dr}$  and  $P$ , (d)  $v_w$ ,  $P_s$ ,  $v_{dc}$  and  $i_{dcr}$ , (e)  $v_{ab}$ ,  $i_{sa}$ ,  $i_{ra}$ ,  $P$ , (f)  $N_r$ ,  $i_{ra}$ ,  $i_{rb}$  and  $i_{rc}$ .
- Fig. 3.32 Dynamic performance of proposed DFIG based WECS under fall in wind speed, (a)  $v_w$ ,  $\omega_r^*$ ,  $\omega_r$  and  $P_s$ , (b)  $i_{dr}^*$ ,  $i_{dr}$ ,  $i_{qr}^*$  and  $i_{qr}$ , (c)  $v_w$ ,  $i_{dr}^*$ ,  $i_{dr}$  and  $P$ , (d)  $v_w$ ,  $P_s$ ,  $v_{dc}$  and  $i_{dcr}$ , (e)  $v_{ab}$ ,  $i_{sa}$ ,  $i_{ra}$ ,  $P$ , (f)  $N_r$ ,  $i_{ra}$ ,  $i_{rb}$  and  $i_{rc}$ .
- Fig. 3.33 Steady state performance of a 3.7kW DFIG at a fixed wind speed of 7 m/sec and at sub-synchronous speed (0.728 pu).
- Fig. 3.34 Steady state performance of a 3.7kW DFIG at a fixed wind speed of 9.2 m/sec and at synchronous speed (1 pu).
- Fig. 3.35 Steady state performance of a 3.7kW DFIG at a fixed wind speed of 12 m/sec and at super - synchronous speed (1.3 pu).
- Fig. 3.36 Dynamic performance of a 3.7kW DFIG at a fixed wind speed of 9.2 m/sec and sudden change in real and reactive power references (1500 rpm to 1835 rpm).
- Fig. 3.37 Dynamic performance of a 3.7kW DFIG for a change in wind speed from 11 m/sec to 8.5 m/sec (1725 to 1390).
- Fig. 3.38 Test results of proposed DPC based DFIG at sub-synchronous speed (0.7 p.u) (a)  $v_{sa}$ ,  $i_{sa}$ ,  $i_{ra}$  and  $N$  (b)  $Q_s$ ,  $P_s$ ,  $\omega_r$  and  $i_{bat}$  (c)  $v_{sa}$ ,  $i_{sa}$ ,  $\sin(\theta_m)_{enc}$  and  $\sin(\theta_m)_{est}$ .
- Fig. 3.39 Test results of proposed DPC based DFIG at synchronous speed (1.0 p.u) (a)  $v_{sa}$ ,  $i_{sa}$ ,  $i_{ra}$  and  $N$  (b)  $Q_s$ ,  $P_s$ ,  $\omega_r$  and  $i_{bat}$  (c)  $v_{sa}$ ,  $i_{sa}$ ,  $\sin(\theta_m)_{enc}$  and  $\sin(\theta_m)_{est}$ .
- Fig. 3.40 Test results of proposed DPC based DFIG at super-synchronous speed (1.1 p.u) (a)  $v_{sa}$ ,  $i_{sa}$ ,  $i_{ra}$  &  $N$  (b)  $Q_s$ ,  $P_s$ ,  $\omega_r$  &  $i_{bat}$  (c)  $v_{sa}$ ,  $i_{sa}$ ,  $\sin(\theta_m)_{enc}$  &  $\sin(\theta_m)_{act}$ .
- Fig. 3.41 Steady state performance of the proposed WECS at fixed wind speed and at a rotor speed of 1300 rpm (a) harmonic spectrum of  $v_{ab}$  (b) harmonic spectrum of  $i_{ga}$  (c) harmonic spectrum of  $i_{gb}$  (d) harmonic spectrum of  $i_{gc}$ .
- Fig. 3.42 Steady state performance of the proposed WECS at fixed wind speed and at a rotor speed of 1500 rpm (a) harmonic spectrum of  $v_{ab}$  (b) harmonic spectrum of  $i_{ga}$  (c) harmonic spectrum of  $i_{gb}$  (d) harmonic spectrum of  $i_{gc}$ .
- Fig. 3.43 Steady state performance of the proposed WECS at fixed wind speed and at a rotor speed of 1700 rpm (a) harmonic spectrum of  $v_{ab}$  (b) harmonic spectrum of  $i_{ga}$  (c) harmonic spectrum of  $i_{gb}$  (d) harmonic spectrum of  $i_{gc}$ .
- Fig. 3.44 Test results of proposed DPC based DFIG for change in active power ( $P_s^*$ ) during constant reactive power ( $Q_s^*$ ) and constant wind speed operation showing (a)  $Q_s^*$ ,  $Q_s$ ,  $P_s^*$  and  $P_s$  during sudden change in  $P_s$ , (b)  $Q_s$ ,  $P_s$ ,  $v_{sa}$  and  $i_{sa}$  during sudden increase in  $P_s$ , (c)  $Q_s$ ,  $P_s$ ,  $v_{sa}$  and  $i_{sa}$  during sudden decrease in  $P_s$  and (d)  $Q_s$ ,  $P_s$ ,  $N$  and  $\omega_r$  during sudden increase in  $P_s$ .
- Fig. 3.45 Test results of proposed DPC based DFIG for change in reactive power ( $Q_s^*$ ) during constant active power ( $P_s^*$ ) and constant wind speed operation showing (a)  $Q_s^*$ ,  $Q_s$ ,  $P_s^*$  and  $P_s$  during sudden change in  $Q_s$ , (b)  $Q_s$ ,  $P_s$ ,  $v_{sa}$  and  $i_{sa}$  during sudden increase in  $Q_s$ , (c)  $Q_s$ ,  $P_s$ ,  $v_{sa}$  and  $i_{sa}$  during sudden decrease in  $Q_s$ .

- Fig. 3.46 Test results of proposed DPC based DFIG for change in wind speed during constant active power ( $P_s^*$ ) and reactive power ( $Q_s^*$ ) (a)  $Q_s$ ,  $P_s$ ,  $\omega_r$  and  $i_{ra}$  (b)  $Q_s$ ,  $P_s$ ,  $\omega_{r(est)}$  and  $\omega_{r(enc)}$ .
- Fig. 3.47 Test results demonstrating the sensorless operation of proposed DPC based DFIG showing (a)  $P_s$ ,  $\sin(\theta_r)$ ,  $\sin(\theta_s)$  and  $\sin(\theta_m)_{est}$  during steady state operation, (b)  $\sin(\theta_m)_{act}$ ,  $\sin(\theta_r)$ ,  $\sin(\theta_s)$  and  $\sin(\theta_m)_{est}$  during steady state operation (c)  $Q_s$ ,  $P_s$ ,  $\sin(\theta_m)_{est}$  and  $\sin(\theta_m)_{act}$  during sudden change in  $P_s$ .
- Fig. 4.1 System configuration of DFIG based grid interfaced WECS.
- Fig. 4.2 Complete control scheme of grid interfaced DFIG for variable speed WECS in both UPF and VR modes.
- Fig. 4.3 MATLAB model of a Single VSC Based Grid Interfaced DFIG for Variable Speed WECS with vector control.
- Fig. 4.4 MATLAB model of a vector control algorithm for RSC.
- Fig. 4.5 MATLAB model of a vector control algorithm for GSC.
- Fig. 4.6 Steady state Performance of proposed DFIG based WECS at super-synchronous speed at 10.8 m/sec wind speed (1.18 pu).
- Fig. 4.7 Steady state Performance of proposed DFIG based WECS at synchronous speed at 9.2 m/sec wind speed (1 pu).
- Fig. 4.8 Steady state Performance of proposed DFIG based WECS at sub-synchronous speed at 8.4 m/sec wind speed (0.92 pu).
- Fig. 4.9 Waveform and harmonic spectrum of grid current ( $i_{ga}$ ) at (a) super-synchronous speed (1.3 pu) and (b) synchronous speed (1 pu).
- Fig. 4.10 Dynamic performance of grid interfaced DFIG at varying wind speeds from 11.5 m/sec to 8.5 m/sec.
- Fig. 4.11 Steady state performance of the proposed WECS at fixed wind speed 10.8 m/sec and at a rotor speed of 1774 rpm. (a)  $v_{ab}$  and  $i_{ga}$ , (b)  $v_{ab}$  and  $i_{gb}$ , (c)  $v_{ab}$  and  $i_{gc}$ , (d)  $v_{ab}$  and  $i_{sa}$ , (e)  $v_{ab}$  and  $i_{sb}$ , (f)  $v_{ab}$  and  $i_{sc}$ , (g)  $v_{ab}$  and  $i_{gsca}$ , (h)  $v_{ab}$  and  $i_{gs cb}$  and (i)  $v_{ab}$  and  $i_{gscc}$ .
- Fig. 4.12 Steady state performance of the proposed WECS at fixed wind speed 10.8 m/sec and at a rotor speed of 1774 rpm (a) grid power ( $P_g$ ), (b) stator power ( $P_s$ ), (c) GSC power ( $P_{gsc}$ ), (d) harmonic spectra of  $i_{ga}$ , (e) harmonic spectra of  $i_{gb}$ , (f) harmonic spectra of  $i_{gc}$ , (g) harmonic spectra of  $i_{sa}$ , (h) harmonic spectra of  $i_{sb}$  and (i) harmonic spectra of  $i_{sc}$ .
- Fig. 4.13 Steady state performance of the proposed WECS at fixed wind speed 9.2 m/sec and at a rotor speed of 1500 rpm. (a)  $v_{ab}$  and  $i_{ga}$ , (b)  $v_{ab}$  and  $i_{gb}$ , (c)  $v_{ab}$  and  $i_{gc}$ , (d)  $v_{ab}$  and  $i_{sa}$ , (e)  $v_{ab}$  and  $i_{sb}$ , (f)  $v_{ab}$  and  $i_{sc}$ , (g)  $v_{ab}$  and  $i_{gsca}$ , (h)  $v_{ab}$  and  $i_{gs cb}$  and (i)  $v_{ab}$  and  $i_{gscc}$ .
- Fig. 4.14 Steady state performance of the proposed WECS at fixed wind speed 9.2 m/sec and at a rotor speed of 1500 rpm (a) grid power ( $P_g$ ), (b) stator power ( $P_s$ ), (c) GSC power ( $P_{gsc}$ ), (d) harmonic spectra of  $i_{ga}$ , (e) harmonic spectra of  $i_{gb}$ , (f) harmonic spectra of  $i_{gc}$ , (g) harmonic spectra of  $i_{sa}$ , (h) harmonic spectra of  $i_{sb}$  and (i) harmonic spectra of  $i_{sc}$ .
- Fig. 4.15 Dynamic performance of proposed DFIG base WECS under rise in wind speed, (a)  $v_w$ ,  $\omega_r^*$ ,  $\omega_r$  and  $P_s$ , (b)  $v_w$ ,  $\omega_r$ ,  $i_{dr}$  and  $i_{qr}$ , (c)  $v_w$ ,  $i_{dgsc}$ ,  $i_{qgsc}$  and  $v_{dc}$ , (d)  $\omega_r$ ,  $P_s$ ,  $P_{gsc}$  and  $P_g$ , (e)  $v_w$ ,  $\omega_r$ ,  $P_g$  and  $Q_g$ .
- Fig. 4.16 Dynamic performance of proposed DFIG base WECS under rise in wind speed, (a)  $\omega_r$ ,  $i_{sa}$ ,  $i_{gsa}$  and  $i_{ga}$ , (b)  $v_w$ ,  $i_{ra}$ ,  $i_{rb}$  and  $i_{rc}$ .

- Fig. 4.17 Dynamic performance of proposed DFIG base WECS under fall in wind speed, (a)  $v_w$ ,  $\omega_r^*$ ,  $\omega_r$  and  $P$ , (b)  $v_w$ ,  $\omega_r$ ,  $i_{dr}$  and  $i_{qr}$ , (c)  $v_w$ ,  $i_{dgsc}$ ,  $i_{qgsc}$  and  $v_{dc}$ , (d)  $\omega_r$ ,  $P_s$ ,  $P_{gsc}$  and  $P_g$ , (e)  $v_w$ ,  $\omega_r$ ,  $P_g$  and  $Q_g$ .
- Fig. 4.18 Dynamic performance of proposed DFIG base WECS under fall in wind speed, (a)  $\omega_r$ ,  $i_{sa}$ ,  $i_{gsa}$  and  $i_{ga}$ , (b)  $v_w$ ,  $i_{ra}$ ,  $i_{rb}$  and  $i_{rc}$ .
- Fig. 4.19 Steady state Performance of proposed DFIG based WECS at super-synchronous speed at 10.8 m/sec wind speed (1.18 pu).
- Fig. 4.20 Steady state Performance of proposed DFIG based WECS at synchronous speed at 9.2 m/sec wind speed (1 pu).
- Fig. 4.21 Steady state Performance of proposed DFIG based WECS at sub-synchronous speed at 8.4 m/sec wind speed (0.92 pu).
- Fig. 4.22 Waveform and harmonic spectrum of grid current ( $i_{ga}$ ) at (a) synchronous speed and (b) super-synchronous speed.
- Fig. 4.23 Dynamic performance of proposed DFIG based WECS at varying wind speeds from 11.5 m/sec to 8.5 m/sec.
- Fig. 4.24 Steady state performance of the proposed WECS at fixed wind speed 10.8 m/sec and at a rotor speed of 1774 rpm. (a)  $v_{ab}$  and  $i_{ga}$ , (b)  $v_{ab}$  and  $i_{gb}$ , (c)  $v_{ab}$  and  $i_{gc}$ , (d)  $v_{ab}$  and  $i_{sa}$ , (e)  $v_{ab}$  and  $i_{sb}$ , (f)  $v_{ab}$  and  $i_{sc}$ , (g)  $v_{ab}$  and  $i_{gsca}$ , (h)  $v_{ab}$  and  $i_{gs cb}$  and (i)  $v_{ab}$  and  $i_{gscc}$ .
- Fig. 4.25 Steady state performance of the proposed WECS at fixed wind speed 10.8 m/sec and at a rotor speed of 1774 rpm (a) grid power ( $P_g$ ), (b) stator power ( $P_s$ ), (c) GSC power ( $P_{gsc}$ ), (d) harmonic spectra of  $i_{ga}$ , (e) harmonic spectra of  $i_{gb}$ , (f) harmonic spectra of  $i_{gc}$ , (g) harmonic spectra of  $i_{sa}$ , (h) harmonic spectra of  $i_{sb}$  and (i) harmonic spectra of  $i_{sc}$ .
- Fig. 4.26 Steady state performance of the proposed WECS at fixed wind speed 9.2 m/sec and at a rotor speed of 1500 rpm. (a)  $v_{ab}$  and  $i_{ga}$ , (b)  $v_{ab}$  and  $i_{gb}$ , (c)  $v_{ab}$  and  $i_{gc}$ , (d)  $v_{ab}$  and  $i_{sa}$ , (e)  $v_{ab}$  and  $i_{sb}$ , (f)  $v_{ab}$  and  $i_{sc}$ , (g)  $v_{ab}$  and  $i_{gsca}$ , (h)  $v_{ab}$  and  $i_{gs cb}$  and (i)  $v_{ab}$  and  $i_{gscc}$ .
- Fig. 4.27 Steady state performance of the proposed WECS at fixed wind speed 9.2 m/sec and at a rotor speed of 1500 rpm (a) grid power ( $P_g$ ), (b) stator power ( $P_s$ ), (c) GSC power ( $P_{gsc}$ ), (d) harmonic spectra of  $i_{ga}$ , (e) harmonic spectra of  $i_{gb}$ , (f) harmonic spectra of  $i_{gc}$ , (g) harmonic spectra of  $i_{sa}$ , (h) harmonic spectra of  $i_{sb}$  and (i) harmonic spectra of  $i_{sc}$ .
- Fig. 4.28 Dynamic performance of proposed DFIG based WECS for the rise in wind speed, (a)  $v_w$ ,  $i_{ds}$ ,  $i_{qs}$  and  $v_{dc}$ , (b)  $v_w$ ,  $\omega_r$ ,  $P_g$  and  $Q_g$ .
- Fig. 4.29 Dynamic performance of proposed DFIG based WECS for the rise in wind speed, (a)  $v_w$ ,  $i_{ds}$ ,  $i_{qs}$  and  $v_{dc}$ , (b)  $v_w$ ,  $\omega_r$ ,  $P_g$  and  $Q_g$ .
- Fig. 5.1 System configuration of grid interfaced DFIG with BESS for regulated output power.
- Fig. 5.2 Complete control scheme of DFIG for grid interfaced WECS with BESS for power smoothening.
- Fig. 5.3 MATLAB model of a single VSC based grid interfaced DFIG for WECS with vector control.
- Fig. 5.4 MATLAB model of a vector control algorithm for RSC.
- Fig. 5.5 MATLAB model of a vector control algorithm for GSC.
- Fig. 5.6 Steady state Performance of proposed DFIG based WECS at super-synchronous speed at 10.8 m/sec wind speed (1.18 pu).

- Fig. 5.7 Steady state Performance of proposed DFIG based WECS at synchronous speed at 9.2 m/sec wind speed (1 pu).
- Fig. 5.8 Steady state Performance of proposed DFIG based WECS at sub-synchronous speed at 8.4 m/sec wind speed (0.92 pu).
- Fig. 5.9 Fig. 5.9 Waveform and harmonic spectrum of grid current ( $i_{ga}$ ) at (a) synchronous speed (1 pu) and (b) super-synchronous speed (1.18 pu).
- Fig. 5.10 Dynamic performance of DFIG for grid interfaced WECS at varying wind speeds from 11.5 m/sec to 8.5 m/sec.
- Fig. 5.11 Steady state performance of the proposed WECS at fixed wind speed 9.2 m/sec and at a rotor speed of 1500 rpm. (a)  $v_{ab}$  and  $i_{ga}$ , (b)  $v_{ab}$  and  $i_{gb}$ , (c)  $v_{ab}$  and  $i_{gc}$ , (d)  $v_{ab}$  and  $i_{sa}$ , (e)  $v_{ab}$  and  $i_{sb}$ , (f)  $v_{ab}$  and  $i_{sc}$ , (g)  $v_{ab}$  and  $i_{gsca}$ , (h)  $v_{ab}$  and  $i_{gs cb}$  and (i)  $v_{ab}$  and  $i_{gscc}$ .
- Fig. 5.12 Steady state performance of the proposed WECS at fixed wind speed 9.2 m/sec and at a rotor speed of 1500 rpm (a) grid power ( $P_g$ ), (b) stator power ( $P_s$ ), (c) GSC power ( $P_{gsc}$ ), (d) harmonic spectra of  $i_{ga}$ , (e) harmonic spectra of  $i_{gb}$ , (f) harmonic spectra of  $i_{gc}$ , (g) harmonic spectra of  $i_{sa}$ , (h) harmonic spectra of  $i_{sb}$  and (i) harmonic spectra of  $i_{sc}$ .
- Fig. 5.13 Steady state performance of the proposed WECS at fixed wind speed 10.8 m/sec and at a rotor speed of 1774 rpm (a)  $v_{ab}$  and  $i_{ga}$ , (b)  $v_{ab}$  and  $i_{gb}$ , (c)  $v_{ab}$  and  $i_{gc}$ , (d)  $v_{ab}$  and  $i_{sa}$ , (e)  $v_{ab}$  and  $i_{sb}$ , (f)  $v_{ab}$  and  $i_{sc}$ , (g)  $v_{ab}$  and  $i_{gsca}$ , (h)  $v_{ab}$  and  $i_{gs cb}$  and (i)  $v_{ab}$  and  $i_{gscc}$ .
- Fig. 5.14 Steady state performance of the proposed WECS at fixed wind 10.8 m/sec and at a rotor speed of 1774 rpm (a) grid power ( $P_g$ ), (b) stator power ( $P_s$ ), (c) GSC power ( $P_{gsc}$ ), (d) harmonic spectra of  $i_{ga}$ , (e) harmonic spectra of  $i_{gb}$ , (f) harmonic spectra of  $i_{gc}$ , (g) harmonic spectra of  $i_{sa}$ , (h) harmonic spectra of  $i_{sb}$  and (i) harmonic spectra of  $i_{sc}$ .
- Fig. 5.15 Dynamic performance of proposed DFIG based WECS under rise in wind speed, (a)  $v_w$ ,  $\omega_r^*$ ,  $\omega_r$  and  $P_s$ , (b)  $v_w$ ,  $\omega_r$ ,  $i_{dr}$  and  $i_{qr}$ , (c)  $\omega_r$ ,  $P_G$ ,  $P_S$  and  $P_{GSC}$ , (d)  $\omega_r$ ,  $i_{b1}$ ,  $i_{b2}$  and  $P_g$ , (e)  $v_{ab}$ ,  $i_{ga}$ ,  $i_{sa}$  and  $i_{gsca}$ , (f)  $\omega_r$ ,  $i_{ra}$ ,  $P_s$  and  $P_G$ .
- Fig. 5.16 Dynamic performance of proposed DFIG based WECS under fall in wind speed, (a)  $v_w$ ,  $\omega_r^*$ ,  $\omega_r$  and  $P$ , (b)  $v_w$ ,  $\omega_r$ ,  $i_{dr}$  and  $i_{qr}$ , (c)  $\omega_r$ ,  $i_{b1}$ ,  $i_{b2}$  and  $P_g$ , (d)  $\omega_r$ ,  $P_G$ ,  $P_S$  and  $P_{GSC}$ , (e)  $v_{ab}$ ,  $i_{ga}$ ,  $i_{sa}$  and  $i_{gsca}$ , (f)  $\omega_r$ ,  $i_{ra}$ ,  $P_s$  and  $P_G$ .
- Fig. 6.1 System Configuration of grid interfaced DFIG with integrated active filter capabilities.
- Fig. 6.2 Complete control scheme of DFIG for grid interfaced WECS with active filter capabilities.
- Fig. 6.3 MATLAB model of a grid interfaced DFIG for WECS with active filter capabilities.
- Fig. 6.4 MATLAB model of a vector control algorithm for RSC.
- Fig. 6.5 MATLAB model of a vector control algorithm for GSC.
- Fig. 6.6 Current waveforms of DFIG based WECS at 12 m/sec wind speed (super-synchronous speed) during steady state.
- Fig. 6.7 Active and reactive powers of DFIG based WECS at 12 m/sec wind speed (super-synchronous speed) during steady state.
- Fig. 6.8 Current waveforms of DFIG based WECS at 12 m/sec wind speed (super-synchronous speed) during steady state.
- Fig. 6.9 Active and reactive powers of DFIG based WECS at 9.2 m/sec wind speed

- (synchronous speed) during steady state.
- Fig. 6.10 Current waveforms of DFIG based WECS at 8.4 m/sec wind speed (sub-synchronous speed) during steady state.
- Fig. 6.11 Active and reactive powers of DFIG based WECS at 8.4 m/sec wind speed (sub-synchronous speed) during steady state.
- Fig. 6.12 Waveform and harmonic spectrum of grid current ( $i_{ga}$ ) at (a) super-synchronous speed (b) synchronous speed and (c) sub-synchronous speed.
- Fig. 6.13 Current waveforms of grid interfaced DFIG based WECS with active filter capabilities for the dynamic changes in wind speeds from 10.5 m/sec to 8.5 m/sec.
- Fig. 6.14 Active and reactive powers of DFIG based grid interfaced WECS with active filter capabilities for the dynamic changes in wind speeds from 10.5 m/sec to 8.5 m/sec.
- Fig. 6.15 Steady state performance of the proposed DFIG based WECS at fixed wind speed of 10.6 m/sec (rotor speed of 1750 rpm (a)  $P_g$ , (b)  $P_s$ , (c)  $P_l$  (d)  $P_{gsc}$ ).
- Fig. 6.16 Steady state performance of the proposed DFIG based WECS at fixed wind speed of 10.6 m/sec (rotor speed of 1750 rpm (a)  $v_{ab}$ ,  $i_{ga}$ , (b)  $v_{ab}$ ,  $i_{gb}$ , (c)  $v_{ab}$ ,  $i_{gc}$ , (d)  $v_{ab}$ ,  $i_{sa}$ , (e)  $v_{ab}$ ,  $i_{sb}$ , (f)  $v_{ab}$ ,  $i_{sc}$ , (g)  $v_{ab}$ ,  $i_{la}$ , (h)  $v_{ab}$ ,  $i_{lb}$ , (i)  $v_{ab}$ ,  $i_{lc}$ , (j)  $v_{ab}$ ,  $i_{gsca}$ , (k)  $v_{ab}$ ,  $i_{gsch}$ , (l)  $v_{ab}$ ,  $i_{gscc}$ ).
- Fig. 6.17 Steady state performance of the proposed DFIG based WECS at fixed wind speed of 8.8 m/sec (rotor speed of 1400 rpm (a)  $i_{ga}$  THD, (b)  $i_{gb}$  THD, (c)  $i_{gc}$  THD, (d)  $i_{sa}$  THD, (e)  $i_{sb}$  THD, (f)  $i_{sc}$  THD, (g)  $i_{la}$  THD, (h)  $i_{lb}$  THD, (i)  $i_{lc}$  THD).
- Fig. 6.18 Steady state performance of the proposed DFIG based WECS working as a Dstatcom at zero wind speed (a)  $v_{ab}$ ,  $i_{ga}$ , (b)  $v_{ab}$ ,  $i_{gb}$ , (c)  $v_{ab}$ ,  $i_{gc}$ , (d)  $v_{ab}$ ,  $i_{la}$ , (e)  $v_{ab}$ ,  $i_{lb}$ , (f)  $v_{ab}$ ,  $i_{lc}$ , (g)  $v_{ab}$ ,  $i_{gsca}$ , (h)  $v_{ab}$ ,  $i_{gsch}$ , (i)  $v_{ab}$ ,  $i_{gscc}$ ).
- Fig. 6.19 Steady state performance of the proposed DFIG based WECS working as a Dstatcom at zero wind speed (a)  $P_g$ , (b)  $P_l$  (c)  $P_{gsc}$ ).
- Fig. 6.20 Steady state performance of the proposed DFIG based WECS working as a Dstatcom at zero wind speed (a)  $i_{la}$  THD, (b)  $i_{lb}$  THD, (c)  $i_{lc}$  THD (d)  $i_{ga}$  THD, (e)  $i_{gb}$  THD, (f)  $i_{gc}$  THD).
- Fig. 6.21 Dynamic performance of DFIG for the rise in wind speed, (a)  $v_w, \omega_r^*, \omega_r$  and  $i_{dr}$ , (b)  $i_{dr}$ ,  $i_{qr}$ ,  $P_s$ , and  $Q_s$ , (c)  $P_s$ ,  $P_{fe}$ ,  $P_l$  and  $P_g$  (d)  $\omega_r^*$ ,  $i_{ra}$ ,  $i_{rb}$  and  $i_{rc}$ ).
- Fig. 6.22 Dynamic performance of DFIG based WECS for the fall in wind speed, (a)  $v_w, \omega_r^*, \omega_r$  and  $i_{dr}$ , (b)  $i_{dr}$ ,  $i_{qr}$ ,  $P_s$ , and  $Q_s$ , (c)  $P_s$ ,  $P_{fe}$ ,  $P_l$  and  $P_g$  (d)  $\omega_r^*$ ,  $i_{ra}$ ,  $i_{rb}$  and  $i_{rc}$ ).
- Fig. 6.23 Dynamic performance of DFIG based WECS for the sudden removal of one phase of local load (a)  $i_{la}$ ,  $i_{la}$ ,  $i_{la}$ , and  $V_{dc}$ , (b)  $i_{la}$ ,  $i_{gsca}$ ,  $i_{sa}$ , and  $i_{ga}$ , (c)  $i_{la}$ ,  $i_{gsca}$ ,  $i_{gsch}$ , and  $i_{gscc}$ , (d)  $i_{la}$ ,  $i_{ga}$ ,  $i_{gb}$ , and  $i_{gc}$ , (e)  $i_{la}$ ,  $i_{sa}$ ,  $i_{sb}$ , and  $i_{sc}$ ).
- Fig. 6.24 Dynamic performance of DFIG based WECS for the sudden injection of one phase of local load, (a)  $i_{la}$ ,  $i_{la}$ ,  $i_{la}$ , and  $V_{dc}$ , (b)  $i_{la}$ ,  $i_{gsca}$ ,  $i_{sa}$ , and  $i_{ga}$ , (c)  $i_{la}$ ,  $i_{gsca}$ ,  $i_{gsch}$ , and  $i_{gscc}$ , (d)  $i_{la}$ ,  $i_{ga}$ ,  $i_{gb}$ , and  $i_{gc}$ , (e)  $i_{la}$ ,  $i_{sa}$ ,  $i_{sb}$ , and  $i_{sc}$ ).
- Fig. 7.1 System Configuration of grid interfaced DFIG with power smoothing and integrated active filter capabilities.
- Fig. 7.2 Complete control scheme of DFIG for grid interfaced WECS with power smoothing and integrated active filter capabilities.
- Fig. 7.3 MATLAB model of a DFIG for grid interfaced WECS with power smoothing and active filter capabilities.
- Fig. 7.4 MATLAB model of a vector control algorithm for RSC.
- Fig. 7.5 MATLAB model of a vector control algorithm for GSC.

- Fig. 7.6 Current waveforms of DFIG based WECS with power smoothening and active filter capabilities at 12 m/sec wind speed (super-synchronous speed) during steady state.
- Fig. 7.7 Active and reactive powers of DFIG based WECS with power smoothening and active filter capabilities at 12 m/sec wind speed (super-synchronous speed) during steady state.
- Fig. 7.8 Current waveforms of DFIG based WECS with power smoothening and active filter capabilities at 9.2 m/sec wind speed (super-synchronous speed) during steady state.
- Fig. 7.9 Active and reactive powers of DFIG based WECS with power smoothening and active filter capabilities at 9.2 m/sec wind speed (synchronous speed) during steady state.
- Fig. 7.10 Current waveforms of DFIG based WECS with power smoothening and active filter capabilities at 8 m/sec wind speed (sub-synchronous speed) during steady state.
- Fig. 7.11 Active and reactive powers of DFIG based WECS with power smoothening and active filter capabilities at 8 m/sec wind speed (sub-synchronous speed) during steady state.
- Fig. 7.12 Fig. 7.12 Waveforms and harmonic spectra of grid current ( $i_{ga}$ ) at (a) super-synchronous speed (b) synchronous speed and (c) sub-synchronous speed.
- Fig. 7.13 Current waveforms of grid interfaced DFIG based WECS with power smoothening and active filter capabilities for the dynamic changes in wind speeds from 10.5 m/sec to 8.5 m/sec.
- Fig. 7.14 Active and reactive powers of DFIG for grid interfaced WECS with power smoothening and active filter capabilities for the dynamic changes in wind speeds from 10.5 m/sec to 8.5 m/sec.
- Fig. 7.15 Steady state performance of the proposed DFIG based WECS at a fixed wind speed of 10.6 m/sec (rotor speed of 1750 rpm) (a)  $v_{ab}$ ,  $i_{ga}$ , (b)  $v_{ab}$ ,  $i_{gb}$ , (c)  $v_{ab}$ ,  $i_{gc}$ , (d)  $v_{ab}$ ,  $i_{sa}$ , (e)  $v_{ab}$ ,  $i_{sb}$ , (f)  $v_{ab}$ ,  $i_{sc}$ , (g)  $v_{ab}$ ,  $i_{la}$ , (h)  $v_{ab}$ ,  $i_{lb}$ , (i)  $v_{ab}$ ,  $i_{lc}$ , (j)  $v_{ab}$ ,  $i_{gsca}$ , (k)  $v_{ab}$ ,  $i_{gs cb}$ , (l)  $v_{ab}$ ,  $i_{gscc}$ .
- Fig. 7.16 Steady state performance of the proposed DFIG based WECS at fixed wind speed of 10.6 m/sec (rotor speed of 1750 rpm) (a)  $P_g$ , (b)  $P_s$ , (c)  $P_l$  (d)  $P_{gsc}$ .
- Fig. 7.17 Steady state performance of the proposed DFIG based WECS at fixed wind speed of 10.6 m/sec (rotor speed of 1750 rpm) (a)  $i_{ga}$  THD, (b)  $i_{gb}$  THD, (c)  $i_{gc}$  THD, (d)  $i_{sa}$  THD, (e)  $i_{sb}$  THD, (f)  $i_{sc}$  THD.
- Fig. 7.18 Steady state performance of the proposed DFIG based WECS working as a Dstatcom at zero wind speed (a)  $P_g$ , (b)  $P_l$  (c)  $P_{gsc}$ .
- Fig. 7.19 Steady state performance of the proposed DFIG based WECS working as a Dstatcom at zero wind speed (a)  $v_{ab}$ ,  $i_{ga}$ , (b)  $v_{ab}$ ,  $i_{gb}$ , (c)  $v_{ab}$ ,  $i_{gc}$ , (d)  $v_{ab}$ ,  $i_{la}$ , (e)  $v_{ab}$ ,  $i_{lb}$ , (f)  $v_{ab}$ ,  $i_{lc}$ , (g)  $v_{ab}$ ,  $i_{gsca}$ , (h)  $v_{ab}$ ,  $i_{gs cb}$ , (i)  $v_{ab}$ ,  $i_{gscc}$ .
- Fig. 7.20 Fig. 7.20 Steady state performance of the proposed DFIG based WECS working as a Dstatcom at zero wind speed (a) harmonic spectrum of  $i_{la}$ , (b) harmonic spectrum of  $i_{lb}$ , (c) harmonic spectrum of  $i_{lc}$  (d) harmonic spectrum of  $i_{ga}$ , (e) harmonic spectrum of  $i_{gb}$  and (f) harmonic spectrum of  $i_{gc}$ .
- Fig. 7.21 Dynamic performance of DFIG for the rise in wind speed, (a)  $v_w, \omega_r^*, \omega_r$  and  $i_{dr}$ , (b)  $i_{dr}$ ,  $i_{qr}$ ,  $P_s$ , and  $Q_s$ , (c)  $P_s$ ,  $P_{fe}$ ,  $P_l$  and  $P_g$  (d)  $\omega_r^*$ ,  $i_{ra}$ ,  $i_{rb}$  and  $i_{rc}$ .

- Fig. 7.22 Dynamic performance of DFIG based WECS for the fall in wind speed, (a)  $v_w, \omega_r^*, \omega_r$  and  $i_{dr}$ , (b)  $i_{dr}, i_{qr}, P_s$  and  $Q_s$ , (c)  $P_s, P_{fe}, P_l$  and  $P_g$  (d)  $\omega_r^*, i_{ra}, i_{rb}$  and  $i_{rc}$ .
- Fig. 7.23 Dynamic performance of DFIG based WECS for the sudden removal of one phase of local load (a)  $i_{la}, \dot{i}_{la}, \ddot{i}_{la}$ , and  $V_{dc}$ , (b)  $i_{la}, i_{fea}, i_{feb}$ , and  $i_{fec}$ , (c)  $i_{la}, i_{fea}, i_{sa}$ , and  $i_{ga}$ , (d)  $i_{la}, i_{ga}, i_{gb}$ , and  $i_{gc}$ , (e)  $i_{la}, i_{sa}, i_{sb}$ , and  $i_{sc}$ .
- Fig. 7.24 Dynamic performance of DFIG based WECS for the sudden injection of one phase of local load, (a)  $i_{la}, \dot{i}_{la}, \ddot{i}_{la}$ , and  $V_{dc}$ , (b)  $i_{la}, i_{fea}, i_{feb}$ , and  $i_{fec}$ , (c)  $i_{la}, i_{fea}, i_{sa}$ , and  $i_{ga}$ , (d)  $i_{la}, i_{ga}, i_{gb}$ , and  $i_{gc}$ , (e)  $i_{la}, i_{sa}, i_{sb}$ , and  $i_{sc}$ .
- Fig. 8.1 System Configuration of standalone DFIG for WECS.
- Fig. 8.2 Complete control scheme of DFIG based SWECS.
- Fig. 8.3 Block diagram of Enhanced Phase Locked Loop (EPLL).
- Fig. 8.4 MATLAB based model of a DFIG for a SWECS.
- Fig. 8.5 MATLAB model of a RSC control algorithm.
- Fig. 8.6 MATLAB model of a LSC control algorithm.
- Fig. 8.7 Simulated performance of DFIG based SWECS under linear loads at fixed wind speed 8.5 m/s.
- Fig. 8.8 Simulated performance of for DFIG based SWECS under nonlinear loads at fixed wind speed 7.5 m/s.
- Fig. 8.9 Waveform and harmonic spectrum of (a) stator current ( $i_{sa}$ ), (b) phase voltage ( $v_a$ ) and (c) load current ( $i_{la}$ ).
- Fig. 8.10 Steady state performance of the proposed DFIG based WECS at a rotor speed of 1820 rpm (super-synchronous) (a)  $v_{ab}, i_{la}$ , (b)  $v_{ab}, i_{lb}$ , (c)  $v_{ab}, i_{lc}$ , (d)  $v_{ab}, i_{sa}$ , (e)  $v_{ab}, i_{sb}$ , (f)  $v_{ab}, i_{sc}$ , (g)  $v_{ab}, i_{sta}$ , (h)  $v_{ab}, i_{stb}$ , (i)  $v_{ab}, i_{stc}$ , (j)  $P_l$ , (k)  $P_s$ , (l)  $P_{st}$ .
- Fig. 8.11 Fig. 8.11 Steady state performance of the proposed DFIG based WECS at a rotor speed of 1820 rpm (super-synchronous) (a) harmonic spectrum of  $i_{la}$ , (b) harmonic spectrum of  $i_{lb}$ , (c) harmonic spectrum of  $i_{lc}$ , (d) harmonic spectrum of  $i_{sa}$ , (e) harmonic spectrum of  $i_{sb}$ , (f) harmonic spectrum of  $i_{sc}$  and (g) harmonic spectrum of  $v_{ab}$ .
- Fig. 8.12 Experimental performance of proposed SWECS during load removal in phase “A” (a)  $v_{ab}, i_{la}, i_{lb}$  and  $i_{lc}$ , (b)  $v_{ab}, i_{sa}, i_{sb}$  and  $i_{sc}$ , (c)  $v_{ab}, i_{sta}, i_{stb}$  and  $i_{stc}$ , (d)  $v_{ab}$  with  $i_{sa}, i_{sta}$  and  $i_{la}$ , (e)  $i_{la}, v_{ab}, v_{bc}$  and  $v_{ca}$  and (d)  $v_{ab}, i_{la}, i_{ra}$  and  $v_{dc}$ .
- Fig. 8.13 Experimental performance of proposed SWECS during load removal in phase “A” (a)  $v_{ab}, i_{la}, i_{lb}$  and  $i_{lc}$ , (b)  $v_{ab}, i_{sa}, i_{sb}$  and  $i_{sc}$ , (c)  $v_{ab}, i_{sta}, i_{stb}$  and  $i_{stc}$ , (d)  $v_{ab}$  with  $i_{sa}, i_{sta}$  and  $i_{la}$ , (e)  $i_{la}, v_{ab}, v_{bc}$  and  $v_{ca}$  and (d)  $v_{ab}, i_{la}, i_{ra}$  and  $v_{dc}$ .
- Fig. 8.14 Steady state performance of the proposed DFIG based WECS at a rotor speed of 1400 rpm (sub-synchronous) (a)  $v_{ab}, i_{la}$ , (b)  $v_{ab}, i_{lb}$ , (c)  $v_{ab}, i_{lc}$ , (d)  $v_{ab}, i_{sa}$ , (e)  $v_{ab}, i_{sb}$ , (f)  $v_{ab}, i_{sc}$ , (g)  $v_{ab}, i_{sta}$ , (h)  $v_{ab}, i_{stb}$ , (i)  $v_{ab}, i_{stc}$ , (j)  $P_l$ , (k)  $P_s$ , (l)  $P_{st}$ .
- Fig. 8.15 Fig. 8.15 Steady state performance of the proposed DFIG based WECS at a rotor speed of 1400 rpm (sub-synchronous) (a) harmonic spectrum of  $i_{la}$ , (b) harmonic spectrum of  $i_{lb}$ , (c) harmonic spectrum of  $i_{lc}$ , (d) harmonic spectrum of  $i_{sa}$ , (e) harmonic spectrum of  $i_{sb}$ , (f) harmonic spectrum of  $i_{sc}$  and (g) harmonic spectrum of  $v_{ab}$ .
- Fig. 8.16 Experimental performance of proposed SWECS during load removal in phase “A” (a)  $v_{ab}, i_{la}, i_{lb}$  and  $i_{lc}$ , (b)  $v_{ab}, i_{sa}, i_{sb}$  and  $i_{sc}$ , (c)  $v_{ab}, i_{sta}, i_{stb}$  and  $i_{stc}$ , (d)  $v_{ab}$  with  $i_{sa}, i_{sta}$  and  $i_{la}$ , (e)  $i_{la}, v_{ab}, v_{bc}$  and  $v_{ca}$  and (d)  $v_{dc}, i_{la}, i_{sa}$  and  $i_{ra}$ .
- Fig. 8.17 Experimental performance of proposed SWECS during load removal in phase “A”

- (a)  $v_{ab}$ ,  $i_{la}$ ,  $i_{lb}$  and  $i_{lc}$ , (b)  $v_{ab}$ ,  $i_{sa}$ ,  $i_{sb}$  and  $i_{sc}$ , (c)  $v_{ab}$ ,  $i_{sta}$ ,  $i_{stb}$  and  $i_{stc}$ , (d)  $v_{ab}$  with  $i_{sa}$ ,  $i_{sta}$  and  $i_{la}$ , (e)  $i_{la}$ ,  $v_{ab}$ ,  $v_{bc}$  and  $v_{ca}$  and (d)  $v_{dc}$ ,  $i_{la}$ ,  $i_{sa}$  and  $i_{ra}$ .
- Fig. 8.18 Experimental performance of proposed SWECS for the dynamic load (a)  $v_{ab}$ ,  $i_{la}$ ,  $i_{lb}$  and  $i_{lc}$ , (b)  $v_{ab}$  with  $i_{sa}$ ,  $i_{sta}$  and  $i_{la}$  and (c)  $v_t$ ,  $i_{la}$ ,  $i_{ra}$  and  $i_{sa}$ .
- Fig. 8.19 Dynamic performance of proposed SWECS under rise in wind speed, (a)  $\omega_r^*$ ,  $v_{ab}$ ,  $i_{sa}$  and  $i_{Ta}$  (b)  $\omega_r^*$ ,  $v_{ab}$ ,  $i_{sa}$  and  $i_{sta}$ .
- Fig. 9.1 System Configuration of single VSC based DFIG for SWECS.
- Fig. 9.2 RSC control algorithm of single VSC based DFIG for SWECS.
- Fig. 9.3 MATLAB model of single VSC based DFIG for SWECS.
- Fig. 9.4 RSC control algorithm of single VSC based DFIG for SWCS.
- Fig. 9.5 Simulated performance of single VSC based DFIG for SWECS under linear loads at a fixed wind speed of 9 m/sec (sub-synchronous speed).
- Fig. 9.6 Simulated performance of single VSC based DFIG for SWECS under linear loads at fixed wind speed of 9 m/s (super-synchronous speed).
- Fig. 9.7 Simulated performance of single VSC based DFIG for SWECS under sudden change in linear consumer loads at fixed wind speed of 9 m/s.
- Fig. 9.8 Simulated performance of single VSC based DFIG for SWECS for a dynamic change in wind speed under linear consumer loads.
- Fig. 9.9 Waveform and harmonic spectra of (a) phase voltage ( $v_a$ ), (b) load current ( $i_{la}$ ).
- Fig. 9.10 Experimental performance of single VSC based DFIG for SWECS at a rotor speed of 1400 rpm (sub-synchronous) (a)  $v_{ab}$ ,  $i_{la}$ , (b)  $v_{ab}$ ,  $i_{lb}$ , (c)  $v_{ab}$ ,  $i_{lc}$ , (d)  $P_l$ , (e)  $v_{dc}$ ,  $i_{br}$ , (f)  $v_{ab}$  THD, (g)  $i_{la}$  THD, (h)  $i_{lb}$  THD, (i)  $i_{lc}$  THD.
- Fig. 9.11 Experimental performance of single VSC based DFIG for SWECS at a rotor speed of 1750 rpm (super-synchronous) (a)  $v_{ab}$ ,  $i_{la}$ , (b)  $v_{ab}$ ,  $i_{lb}$ , (c)  $v_{ab}$ ,  $i_{lc}$ , (d)  $P_l$ , (e)  $v_{dc}$ ,  $i_{br}$ , (f)  $v_{ab}$  THD, (g)  $i_{la}$  THD, (h)  $i_{lb}$  THD, (i)  $i_{lc}$  THD.
- Fig. 9.12 Experimental performance of single VSC based DFIG for SWECS under sudden increase in linear consumer loads (a)  $v_t^*$ ,  $v_t$ ,  $v_{ab}$  and  $i_{la}$ , (b)  $v_{ab}$ ,  $i_{sa}$ ,  $i_{ra}$  and  $\omega_r$ , (c)  $\omega_r$ ,  $P_s$ ,  $Q_s$  and  $i_{br}$ .
- Fig. 9.13 Experimental performance of single VSC based DFIG for SWECS under sudden decrease in linear consumer loads (a)  $v_t^*$ ,  $v_t$ ,  $v_{ab}$  and  $i_{la}$ , (b)  $v_{ab}$ ,  $i_{sa}$ ,  $i_{ra}$  and  $\omega_r$ , (c)  $\omega_r$ ,  $P_s$ ,  $Q_s$  and  $i_{br}$ .
- Fig. 9.14 Experimental performance of single VSC based DFIG for SWECS under rise in wind speed for a fixed linear consumer loads, (a)  $\omega_r$ ,  $i_{sa}$ ,  $i_{ra}$  and  $v_{ab}$ , (b)  $\omega_r$ ,  $P_s$ ,  $Q_s$  and  $i_{br}$ .
- Fig. 9.15 Experimental performance of single VSC based DFIG for SWECS under rise in wind speed for a fixed linear consumer loads, (a)  $\omega_r$ ,  $i_{sa}$ ,  $i_{ra}$  and  $v_{ab}$ , (b)  $\omega_r$ ,  $P_s$ ,  $Q_s$  and  $i_{dcr}$ .
- Fig. 10.1 System Configuration of DFIG based SWECS with BESS.
- Fig. 10.2 Complete control schematic DFIG based SWECS with BESS.
- Fig. 10.3 Block diagram of Model Reference Adaptive System (MRAS) sensorless algorithm for the DFIG based SWECS with BESS.
- Fig. 10.4 MATLAB model of an overall power circuit of a DFIG based SWECS with BESS.
- Fig. 10.5 MATLAB model of an RSC control algorithm for a DFIG based SWECS.
- Fig. 10.6 MATLAB model of an LSC control algorithm for a DFIG based SWECS.
- Fig. 10.7 MATLAB model of an MRAS based sensorless algorithm for a DFIG based SWECS.

- Fig. 10.8 Simulated performance of DFIG based SWECS with BESS under linear loads at fixed wind speed 8 m/s.
- Fig. 10.9 Simulated performance of DFIG based SWECS with BESS under nonlinear loads at fixed wind speed 11 m/s.
- Fig. 10.10 Waveform and harmonic spectrum of (a) stator current ( $i_{sa}$ ), (b) line voltage ( $v_a$ ), (c) load current ( $i_{la}$ ).
- Fig. 10.11 Simulated performance of DFIG based SWECS with BESS under nonlinear loads for increasing wind speed from 8 m/sec to 11 m/s.
- Fig. 10.12 Steady state performance of the proposed DFIG based WECS under linear load at a rotor speed of 1400 rpm (sub-synchronous) (a)  $v_{ab}$ ,  $i_{la}$ , (b)  $v_{ab}$ ,  $i_{lb}$ , (c)  $v_{ab}$ ,  $i_{lc}$ , (d)  $v_{ab}$ ,  $i_{sa}$ , (e)  $v_{ab}$ ,  $i_{sb}$ , (f)  $v_{ab}$ ,  $i_{sc}$ , (g)  $v_{ab}$ ,  $i_{sta}$ , (h)  $v_{ab}$ ,  $i_{stb}$ , (i)  $v_{ab}$ ,  $i_{stc}$ , (j)  $P_l$ , (k)  $P_s$ , (l)  $P_{st}$ .
- Fig. 10.13 Fig. 10.13 Steady state performance of the proposed DFIG based WECS under linear load at a rotor speed of 1400 rpm (sub-synchronous) (a) harmonic spectrum of  $i_{la}$ , (b) harmonic spectrum of  $i_{lb}$ , (c) harmonic spectrum of  $i_{lc}$ , (d) harmonic spectrum of  $i_{sa}$ , (e) harmonic spectrum of  $i_{sb}$ , (f) harmonic spectrum of  $i_{sc}$  and (g) harmonic spectrum of  $v_{ab}$ .
- Fig. 10.14 Experimental performance of proposed SWECS under linear load during load removal in phase “A” (a)  $v_{ab}$ ,  $i_{la}$ ,  $i_{lb}$  and  $i_{lc}$ , (b)  $v_{ab}$ ,  $i_{sa}$ ,  $i_{sb}$  and  $i_{sc}$ , (c)  $v_{ab}$ ,  $i_{sta}$ ,  $i_{stb}$  and  $i_{stc}$ , (d)  $v_{ab}$ ,  $v_{bc}$ ,  $v_{ca}$  and  $i_{la}$ , (e)  $v_{ab}$ ,  $i_{la}$ ,  $i_{sa}$  and  $i_{sta}$  and (f)  $v_{ab}$ ,  $i_{la}$ ,  $i_{br}$  and  $i_{bs}$ .
- Fig. 10.15 Experimental performance of proposed SWECS under linear load during sudden addition of load in phase “A” (a)  $v_{ab}$ ,  $i_{la}$ ,  $i_{lb}$  and  $i_{lc}$ , (b)  $v_{ab}$ ,  $i_{sa}$ ,  $i_{sb}$  and  $i_{sc}$ , (c)  $v_{ab}$ ,  $i_{sta}$ ,  $i_{stb}$  and  $i_{stc}$ , (d)  $v_{ab}$ ,  $v_{bc}$ ,  $v_{ca}$  and  $i_{la}$ , (e)  $v_{ab}$ ,  $i_{la}$ ,  $i_{sa}$  and  $i_{sta}$  and (f)  $v_{ab}$ ,  $i_{la}$ ,  $i_{br}$  and  $i_{bs}$ .
- Fig. 10.16 Steady state performance of the proposed DFIG based WECS at a rotor speed of 1400 rpm (sub-synchronous) (a)  $v_{ab}$ ,  $i_{la}$ , (b)  $v_{ab}$ ,  $i_{lb}$ , (c)  $v_{ab}$ ,  $i_{lc}$ , (d)  $v_{ab}$ ,  $i_{sa}$ , (e)  $v_{ab}$ ,  $i_{sb}$ , (f)  $v_{ab}$ ,  $i_{sc}$ , (g)  $v_{ab}$ ,  $i_{sta}$ , (h)  $v_{ab}$ ,  $i_{stb}$ , (i)  $v_{ab}$ ,  $i_{stc}$ , (j)  $P_l$ , (k)  $P_s$ , (l)  $P_{st}$ .
- Fig. 10.17 Steady state performance of the proposed DFIG based WECS at a rotor speed of 1400 rpm (sub-synchronous) (a)  $i_{la}$  THD, (b)  $i_{lb}$  THD, (c)  $i_{lc}$  THD, (d)  $i_{sa}$  THD, (e)  $i_{sb}$  THD, (f)  $i_{sc}$  THD and (g)  $v_{ab}$  THD.
- Fig. 10.18 Experimental performance of proposed SWECS during load removal in phase “A” (a)  $v_{ab}$ ,  $i_{la}$ ,  $i_{lb}$  and  $i_{lc}$ , (b)  $v_{ab}$ ,  $i_{sta}$ ,  $i_{stb}$  and  $i_{stc}$  (c)  $v_{ab}$  with  $i_{sa}$ ,  $i_{sta}$  and  $i_{la}$ , (d)  $v_{dc}$ ,  $i_{la}$ ,  $i_{sa}$  and  $i_{ra}$ .
- Fig. 10.19 Experimental performance of proposed SWECS during load removal in phase “A” (a)  $v_{ab}$ ,  $i_{la}$ ,  $i_{lb}$  and  $i_{lc}$ , (b)  $v_{ab}$  with  $i_{sa}$ ,  $i_{sta}$  and  $i_{la}$ , (c)  $v_{ab}$ ,  $i_{sta}$ ,  $i_{stb}$  and  $i_{stc}$  and (d)  $v_{dc}$ ,  $i_{la}$ ,  $i_{ra}$  and  $i_{sa}$ .
- Fig. 10.20 Experimental performance of proposed SWECS for the dynamic load (a)  $v_{ab}$ ,  $i_{la}$ ,  $i_{sa}$  and  $i_{sta}$ , and (b)  $v_{ab}$  with  $i_{la}$ ,  $i_{sa}$  and  $i_{bs}$ .
- Fig. 10.21 Dynamic performance of proposed SWECS under rise in wind speed, (a)  $v_{\omega}$ ,  $\omega_r^*$ ,  $\omega_r$ ,  $P_s$ , (b)  $v_{\omega}$ ,  $P_s$ ,  $i_{bs}$  and  $i_{br}$ , (c)  $v_{ab}$ ,  $P_s$ ,  $i_{sa}$  and  $i_{ra}$  (d)  $v_{ab}$ ,  $i_{la}$ ,  $i_{sa}$  and  $i_{ra}$ .
- Fig. 10.22 Dynamic performance of proposed SWECS under fall in wind speed, (a)  $v_{\omega}$ ,  $\omega_r^*$ ,  $\omega_r$ ,  $P_s$ , (b)  $v_{\omega}$ ,  $P_s$ ,  $i_{bs}$  and  $i_{br}$ , (c)  $v_{ab}$ ,  $P_s$ ,  $i_{sa}$  and  $i_{ra}$  (d)  $v_{ab}$ ,  $i_{la}$ ,  $i_{sa}$  and  $i_{ra}$ .

## LIST OF TABLES

Table 3.1 Optimal DPC vector selection

Table 5.1 Different power calculations of DFIG at different wind speeds

## LIST OF ABBREVIATIONS

AC	Alternating Current
BESS	Battery Energy Storage System
DC	Direct Current
DFIG	Doubly Fed Induction Generator
DPF	Displacement Power Factor
DSP	Digital Signal Processor
DTC	Direct Torque Control
GSC	Grid Side Converter
LSC	Load Side Converter
MPPT	Maximum Power Point Tracking
MRAS	Model Reference Adaptive System
PCC	Point of Common Coupling
PF	Power Factor
PI	Proportional and Integral
PMSM	Permanent Magnet Synchronous Machine
PWM	Pulse Width Modulation
RSC	Rotor Side Converter
WECS	Standalone Wind Energy Conversion System
STATCOM	Static Compensator
THD	Total Harmonic Distortion
UPF	Unity Power factor
VC	Vector Control
VSC	Voltage Source Converter
WECS	Wind Energy Conversion System
WRIM	Wound Rotor Induction Machine

## LIST OF SYMBOLS

$i_{sa}, i_{sb}, i_{sc}$	Three phase stator currents ( $i_{sabc}$ )
$i_{ra}, i_{rb}, i_{rc}$	Three phase rotor currents( $i_{rabc}$ )
$i_{ga}, i_{gb}, i_{gc}$	Three phase grid currents ( $i_{gabc}$ )
$i_{la}, i_{lb}, i_{lc}$	Three phase load currents ( $i_{labc}$ )
$i_{sta}, i_{stb}, i_{stc}$	LSC currents in standalone WECS
$i_{gsca}, i_{gs cb}, i_{gscc}$	Three phase grid side converter currents ( $i_{gsabc}$ )
$i_{r\alpha}, i_{r\beta}$	Components of rotor currents in rotor co-ordinates
$i_{rsa}, i_{rs\beta}$	Components of rotor currents in stator co-ordinates
$i_{ms}$	Magnetizing current
$i_{ms\alpha}, i_{ms\beta}$	Components of $i_{ms}$ in stator co-ordinates
$i_{sa}, i_{s\beta}$	Components of Stator currents in stator co-ordinates
$i_{dr}^*$	Direct axis rotor reference current
$i_{qr}^*$	Quadrature axis rotor reference current
$i_{dr}$	Direct axis rotor current
$i_{qr}$	Quadrature axis rotor current
$v_{gab}, v_{gbc}, v_{gca}$	Three phase grid line voltages( $v_{gabc}$ )
$v_{ab}, v_{bc}, v_{ca}$	Three phase stator line voltages ( $v_{abc}$ )
$v_r$	Rotor Voltage
$v_{dr}^*$	Direct axis reference rotor voltages
$v_{qr}^*$	Quadrature axis reference rotor voltages
$P_{rmax}$	Maximum rotor active power
$P_g$	Grid Active Power
$P_l$	Load Active Power
$P_s$	Stator Active Power
$P_{gsc}$	GSC Active Power
$P_{st}$	LSC Active Power in standalone WECS
$Q_g$	Grid Reactive Power
$Q_l$	Load Reactive Power

$Q_s$	Stator Reactive Power
$Q_{gsc}$	GSC Reactive Power
$Q_{st}$	LSC Active Power in standalone WECS
$(\omega_r)_{act}$	Actual speed in rad/sec
$(\omega_r)_{est}$	Estimated speed in rad/sec
$N_r$	Actual Speed in rpm
$N_r^*$	Reference Speed in rpm
$V_{dc}$	DC Link voltage or BESS voltage
$v_w$	Wind Speed in m/sec
$\theta_r$	Angle of rotor current vector wrt rotor axis
$\theta_m$	Rotor position (angle of rotor axis wrt stator axis)
$\theta_e$	Angle of stator flux vector wrt stator axis
$\theta$	Angle of stator voltage vector wrt stator axis
$\lambda$	<i>Tip Speed Ratio</i>
$\beta$	<i>Pitch Angle</i>
$S$	<i>Slip</i>
$L_m$	Magnetizing inductance
$\hat{\theta}_r$	estimated rotor position
$S_P$	active power switching states
$S_Q$	Reactive power switching states
$\Psi_{s\alpha}, \Psi_{s\beta}$	stationary frame stator flux linkages
$C_p$	Power Coefficient
$\eta$	Gear box ratio